eJNDT e-Journal of Nondestructive Testing - ISSN 1435-4934 - www.ndt.net

EWGAE 2024
36th Conference of the European Working Group on Acoustic Emission

Development of a Semi-Autonomous Pulse and Receive Concrete Inspection System

Tim ATKINSON [1], Matthew PEARSON [1], John MCCRORY [1], Ryan MARKS [2], Rhys PULLIN [1]
[1] Cardiff University School of Engineering, Cardiff, Wales, AtkinsonT1@cardiff.ac.uk
[2] MISTRAS Group Inc, Bridgend, Wales, Ryan.Marks@MistrasGroup.com

Abstract. Concrete structures are being subjected to increasing loads and used beyond their intended lifespan. When combined with operators shrinking maintenance budgets it is imperative structures are monitored for damage. Acoustic Emission (AE) and AE Tomography offer a method for damage detection and characterisation. However, they are encumbered by their equipment and setup requirements, and best used on areas where damage is already known to have occurred. An autonomous pulse catch system could be used to identify these areas. To explore the potential of such a system, seven concrete beams differentiated by their aggregate size were tested using an automated pulse and receive system. The effect of aggregate size, and pulse frequency on attenuation and wavespeed are investigated. The pulse regime consisted of narrowband pulses ranging from 30 kHz to 500 kHz. The results show that high frequency pulses experienced greater attenuation than low frequency pulses. Whilst a link appears between the size of the aggregate and the rate of attenuation of high frequency signals. A strong negative correlation between amplitude loss and pulse frequency was observed. For the specimen containing coarse aggregate, pulse velocity was constant between 100 kHz and 500 kHz, whereas specimens containing coarse aggregate experienced frequency dependant attenuation. This testing shows the significant potential for an automated pulse and receive system, which could lead to the development of an autonomous health monitoring system. In addition, the approach can be instrumental in developing large data sets, that can be used in Machine Learning processes, to develop a deeper understanding of AE signal propagation in concrete materials.

Keywords: Autonomous Monitoring, Concrete, Frequency, Data-Acquisition

Introduction

Global health monitoring of large concrete structures using AE is a significant challenge. Due to the highly attenuative nature of concrete, and the large geometric spreading that occurs, measuring AE across large distances is difficult. Damage detection and imaging

https://doi.org/10.58286/30247

techniques such as Acoustic Tomography [1] are promising but require significant equipment, setup, and post-processing. In lieu of true global monitoring, smart or autonomous monitoring has the potential to identify areas of damage using minimal equipment and operator input. Once a specific area of damage has been identified, more thorough damage detection and classification can take place.

The relationship between concrete quality and ultrasonic wave speed has long been understood [2] [3]. Work by Park et al. [4] has trained various Machine Learning (ML) algorithms to accurately predict the compressive strength of concrete using Longitudinal, Transverse, and Rayleigh wave speeds. Whilst successful it was found that the mix design of concrete should be used in addition to the ultrasonic velocities. This is expected given that water-content and aggregate size impacts wave speed and attenuation [5] [6].

The goal of this testing is to explore the potential for a 'pulse and receive' test-rig, designed to be mounted to the underside of an autonomous rover for automated collection of AE data across large concrete surfaces. An advantage of pulse and receive is that narrowband pulses can be used to test the response to specific frequencies. This allows for the collection of significantly more data per measurement section than traditional Pencil Lead Breaks (PLBs) [7] or Impact Echo [8].

If the effect of water-content and aggregate on wave properties is better understood, then this can be used to aid in the training of ML algorithms or used to improve the accuracy of imaging techniques. Li et al [9] used water-cement ratio, sand ratio, and aggregate size as parameters in a velocity attenuation model. When applied to location testing this velocity model reduced localisation error.

Without considering what the mix of poured concrete is, an autonomous system taking periodic measurements on a concrete structure would be sensitive to changes in aggregate and water-content. To investigate the impact of these mix factors on a pulse and receive system, seven concrete specimens were produced. Each with identical mix ratios, differing only in the size of aggregate used.

1. Methodology

1.1 Concrete Specimens

Seven plain concrete beams were produced, each measuring 0.5 x 0.1 x 0.1 m. The goal was to produce specimens with a variety of aggregate sizes, whilst keeping the other mix parameters consistent. This posed a challenge as the mix had to be workable across a range of aggregate sizes. A mix ratio of 2.2: 4.3: 5.3 (Concrete: Fine Aggregate: Coarse Aggregate (C_A)) was used. Aggregate was sieved into seven different sizes, 1-2mm, 2-4mm, 4-6mm, 4-10mm, 10-14mm, and 14-20mm. A random sample from each set of aggregate can be seen in Figure 1. Additionally, a sample was mixed containing no C_A. Once hardened the specimens were cured in a water-tank for 22 days. Once removed from the tank the specimens were left to air-dry for 7 days.

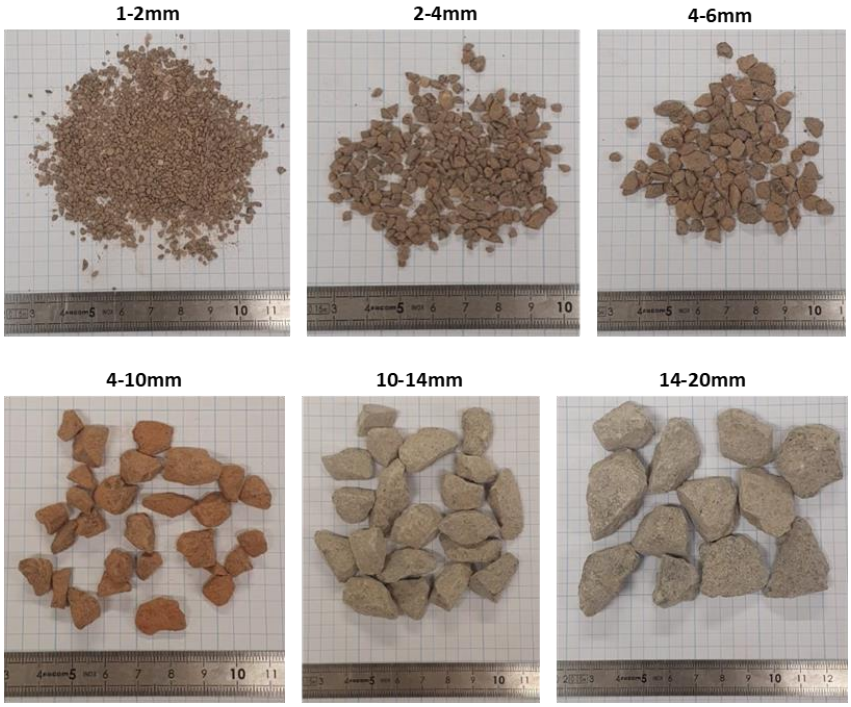

Figure 1 - Photos of a random sample from each set of aggregate.

1.2 Generation and Acquisition of the Pulsed Signals

A STEMlab Red Pitaya 125-14 was used to produce narrowband signals in the form of a 10-oscillation sine wave, this was connected via a 200V pk-pk amplifier to a Conical Transducer [10]. This transducer was used as a 'pulser' to inject artificial ultrasonic waves into the specimen. The Red Pitaya was controlled via its SCPI Python library, and a script was developed to automatically pulse eight repetitions of each frequency in the range of 30 kHz to 500 kHz, in steps of 10 kHz. Preliminary testing showed that typical resonant AE sensors were not effective at producing a narrowband pulse. Despite being driven by a pure frequency signal, the produced pulses were rarely narrowband. The pulses produced were wideband, often dominated by frequencies lower than the source signal.

The Conical Transducer in contrast was able to produce accurate narrowband pulses. This novel transducer contains a spring-loaded cone-shaped piezoelectric element, which can be driven to produce artificial ultrasonic pulses up to 1 MHz [11]. Previous work has made use of this transducer to produce artificial AE sources in plate structures [12].

PAC Wideband Differential (WD) sensors were used to measure the produced pulses, the data was captured using a PAC PCI-2 four Channel AE System running at 5 MHz. The WDs were selected due to their flat frequency response. MISTRAS 2/4/6 pre-amplifiers were used to amplify the WDs, set to a pre-amp gain of 40 dB.

As the pulsed waveforms reduce in duration as the frequency increased, the overall energy of the pulse decreases as the frequency increases. To account for this, two methods of normalizing the energy of the pulses was developed.

The first increased the number of oscillations of the source sine wave to normalize the energy across the whole frequency range. The second adjusted the amplitude of the wave whilst maintaining ten oscillations. Both methods resulted in a consistent source energy across the frequency range. In testing the first normalization method was used, keeping the pulsed energy consistent across the full range of frequencies used.

1.4 Test Process

To produce consistent results for each specimen a test rig was used to hold the receiving sensors and the conical transducer. This allowed for the sensor setup to be transferred quickly between specimens without risk of changing the sensor spacing. The Conical Transducer's sprung sensor face requires the sensor casing be firmly pressed against the specimen. The mounts for the WD receiving sensors were also sprung loaded to ensure good contact. A diagram of the test rig can be seen in Figure 2. The first WD was 45mm from the Conical Transducer (centre to centre), each following sensor was 84mm from the previous.

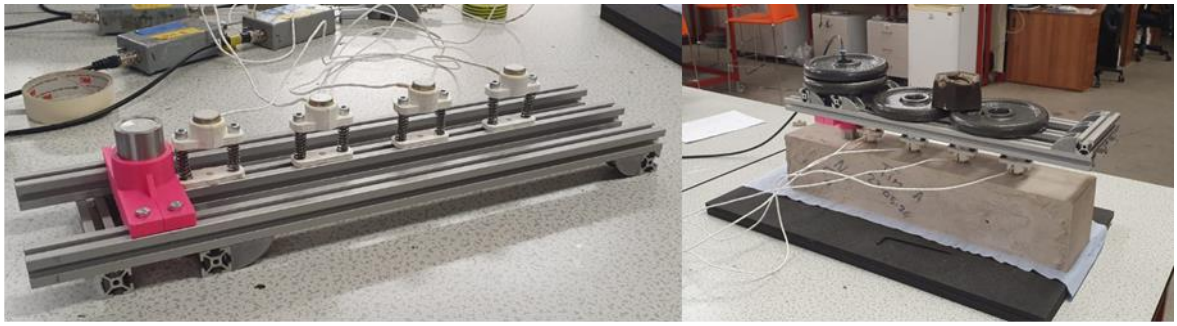

Figure 2 - Left: An image of the test rig inverted. Right: The test rig placed on a specimen for testing.

For each specimen, the surface was lightly sanded and brushed. The test rig was then placed on the prepared surface 100 mm from the end of the specimen, with 6 kg weighing it down. High temperature grease was used as a couplant. To ensure each WD was properly mounted, sensitivity testing was carried out using PLBs.

Once the sensors were confirmed as properly mounted, the Red Pitaya was used to produce pulses from 30 to 500 kHz, in steps of 10 kHz. Each frequency was repeated 8 times. Resulting in a total of 384 AE events, with four AE signals per event, one from each channel. Once the primary testing was competed, eight PLBs were done on the far side of the conical transducer, to provide comparative data. Figure 3 shows the process for producing and recording the ultrasonic waves.

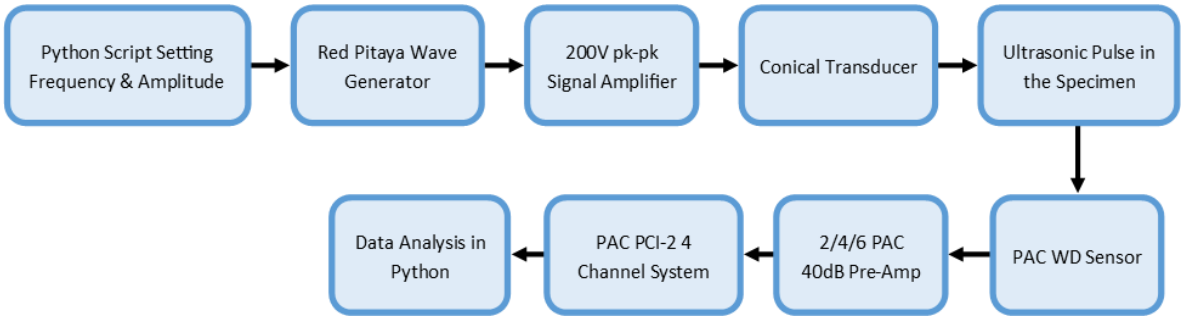

Figure 3- Flowchart showing the signal generation and data acquisition setup.

Wave speed and amplitude were then calculated for each signal and averaged across the eight repeats. An AIC Picker [13][14] was used to determine the time of arrival (TOA) for each hit, wave speed was then calculated for each channel using the TOA difference from Channel 1. An AIC picker was used over a threshold-based picker as with threshold pickers, a decrease in amplitude can lead to erroneous arrival times caused by the increased time required for the waveform to reach the threshold.

2. Results and Discussion

2.1 Comparison of Pulsed Signals to Pencil-Lead-Breaks

Comparing the waveforms (Figure 4) and their associated Fast-Fourier-Transforms (Figure 5) shows the difference between the source types. A notable difference is in the first arrival of the wave. Waves produced using a PLB have an immediate arrival, a rapid rise time with the highest amplitude occurring at the front of the wave. In contrast the waves produced with an artificial pulse have a slower rise time to the highest amplitude followed by a similar size ramp down. The pulse wave is more concentrated with a shorter ring down time, when compared to a PLB. The differences are likely a result of a PLB being an instantaneous release of energy more closely resembling a fracture, whereas the pulse releases the energy over a longer period.

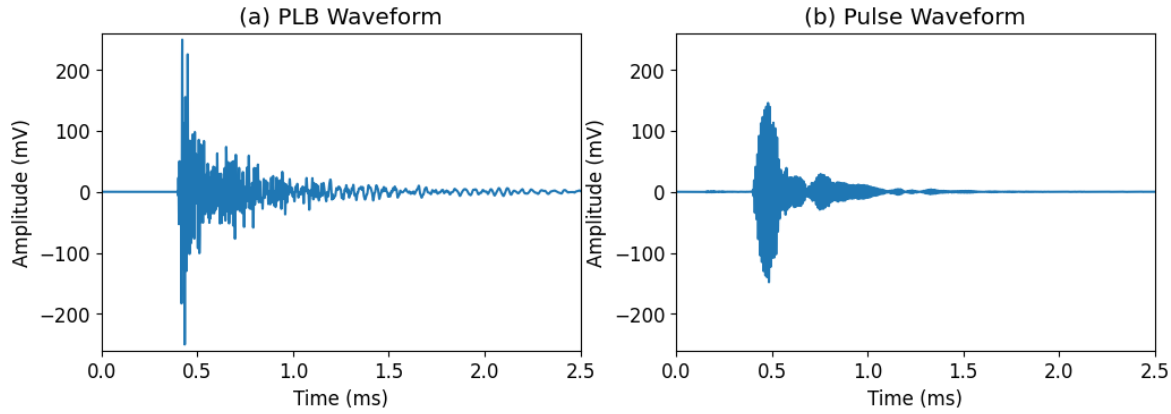

Figure 4 - Raw Waveforms captured by Channel 1 from the 4-6mm Specimen (a) Pencil-Lead-Break Source, (b) Pulsed Waveform produced by the Conical Transducer driven at 100 kHz

Figure 5 below shows the FFTs for the above waveforms, The broadband nature of PLB waveforms is clear in Figure 5(a). Whilst the narrowband behaviour of the pulsed signals is visible in Figure 5 (b). Most of the energy is concentrated about the driving frequency of 100 kHz, showing that the conical transducer has produced a true narrow-band pulse.

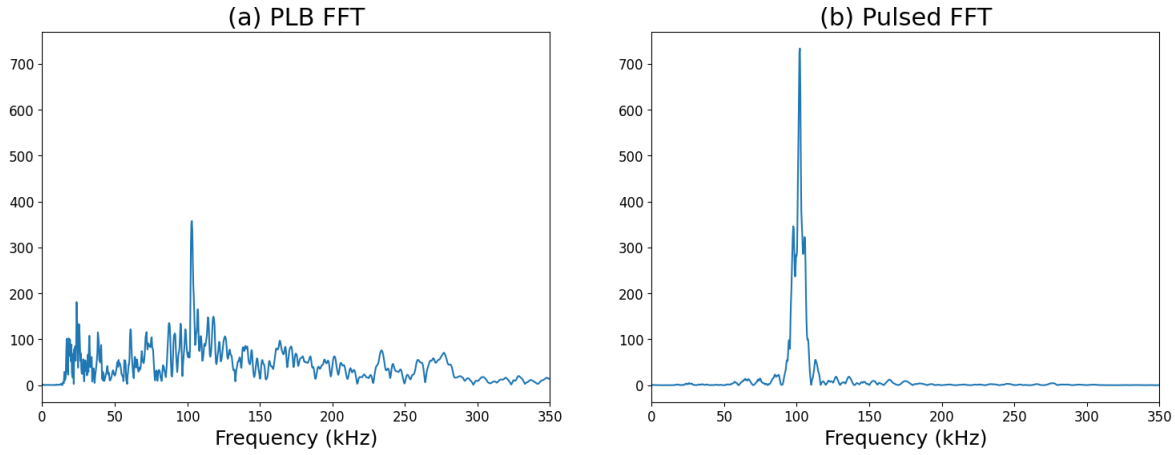

Figure 5 - Raw Waveforms captured by Channel 1 from the 4-6mm Specimen (a) Pencil-Lead-Break Source, (b) Pulsed Waveform produced by the Conical Transducer driven at 100 kHz

2.2 Frequency Components of the Pulse Signal

To ensure that the Conical Transducer was correctly producing narrowband signals across the whole frequency range, the peak frequency of the collected waveforms was plotted against the source signal frequency used to drive the transducer. This can be seen in Figure 6. Looking at Channel 1 which is closest to the source, the Conical Transducer is producing accurate narrow-band waves, with high accuracy at the lower frequencies.

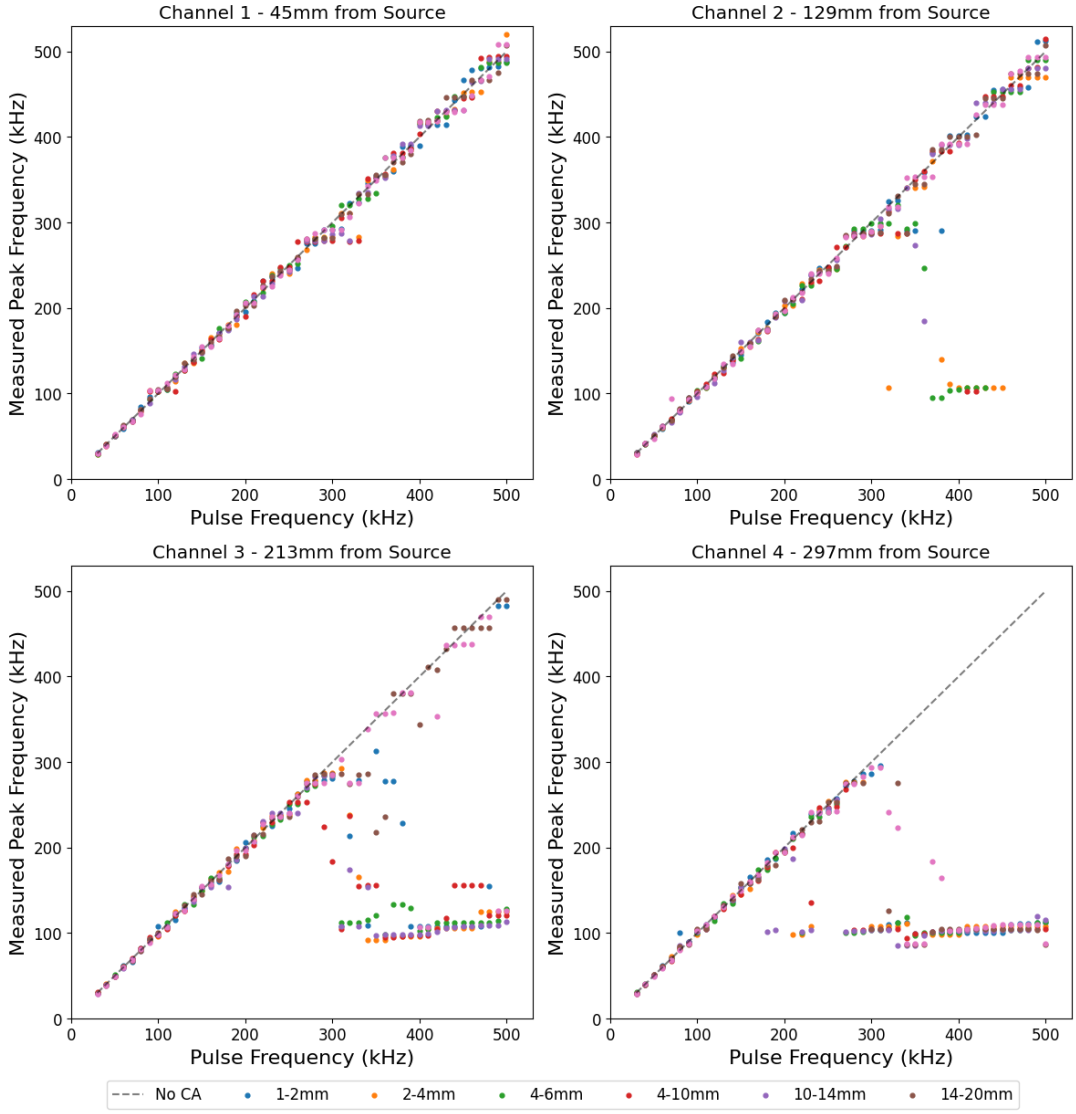

Figure 6 - Measured Peak Frequency plotted against the Source Signal Frequency used to drive the Conical Transducer for each evenly spaced sensor.

As the wave travels through the specimen, the peak frequency decreases to a minimum of 100 kHz. Looking at Channel 2 the smaller aggregate sizes (1-2, 2-4, and 4-6 mm) have reached this minimum for pulses in the 400 kHz range, whilst the larger aggregate sizes appear to maintain the high frequency peaks. By Channel 4 (297 mm) the 100 kHz minimum is clear, with no high frequency pulses remaining. This banding is believed to be caused by the WD receiving sensors, as their operating range is 100-1000 kHz, however the waveforms produced by low source frequencies pulses are not banding at 100 kHz.

This decrease in measured frequency as a function of distance is in line with previous work by Wu et al. [15]. In their work the frequency centroid of PLB induced

waves was found to decrease with distance, similarly to this testing they tested specimens containing a range of aggregates. The testing presented in this paper showed a similar trend, Figure 7 shows an example of this occurring for the 500 kHz pulses produced by the Red Pitaya.

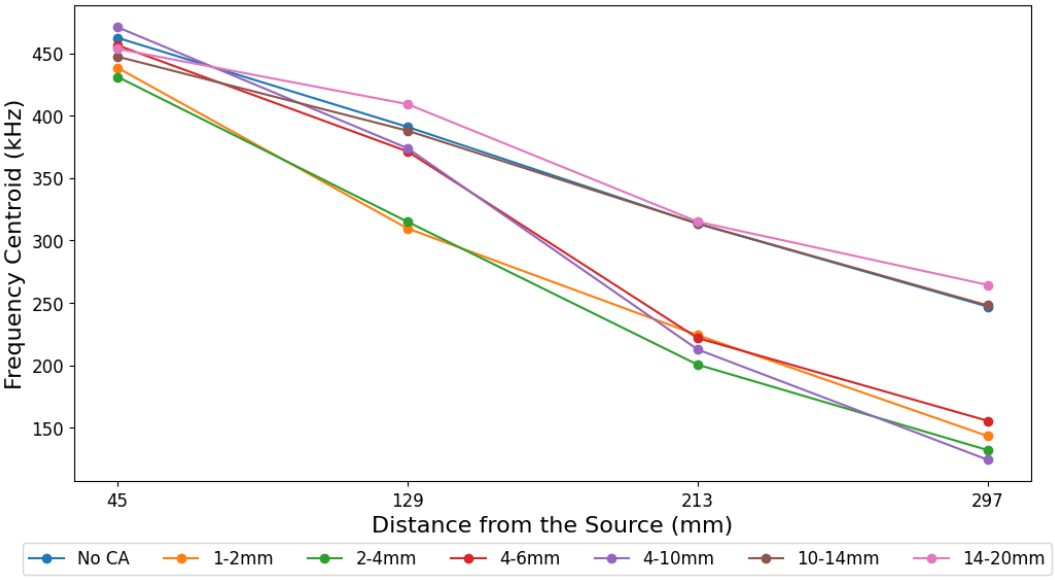

Figure 7 - Frequency Centroid Decay of a 500 kHz pulse, plotted against the distance from the source.

In contrast to the testing by Wu et al. a trend does appear across the aggregate sizes. The large aggregates (10-14 and 14-20 mm) separate from the smaller aggregates. Whilst the medium size aggregates cross over the divide between channel 2 and channel 3. It's thought that frequency attenuation is related to the size of the coarse aggregate.

2.3 Amplitude Decay

Figure 8 shows the amplitude ratio calculated for each frequency pulse. Each point represents an average of eight individual waveforms. As a ratio of the peak amplitude of the first sensor to the last, it's an indicator of the attenuation occurring between Channel 1 and Channel 4.

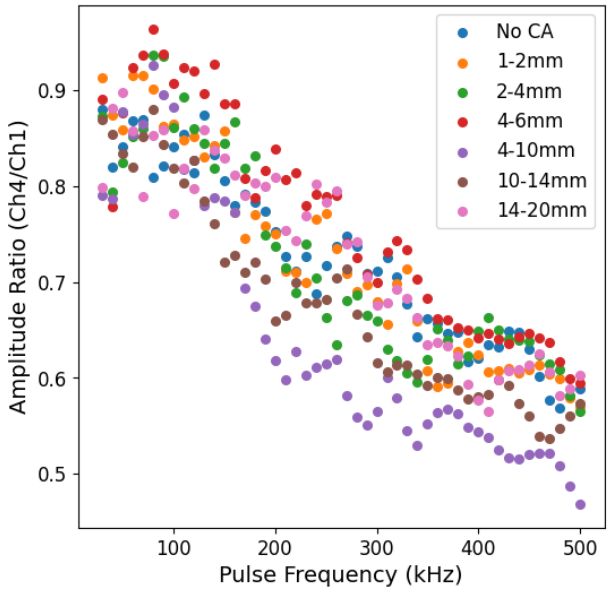

Figure 8 - Ratio of Peak Amplitudes of Channel 4 and Channel 1. An average of 8 iterations.

No clear correlation between aggregate size and amplitude ratio is visible, however a clear negative trend appears. The decrease in amplitude negatively correlates with the pulse frequency. This agrees with Figure 6, in concrete the high frequencies suffer from greater attenuation.

2.4 Pulse Velocity

The individual pulse velocities for each channel are shown below in Figure 9. Two notable features emerge, first is the area of low pulse velocity for the low frequency pulses, second is the No Coarse Aggregate sample maintaining high velocity at greater distance, as shown by Channel 4. This suggests that the coarse aggregate is responsible for the reduction in pulse velocity at high frequencies. This relationship could be used to identify areas of concrete where aggregate is expected but not present. This can occur in specimens or mixes containing large aggregate, where excessive vibration can lead to the aggregate sinking in the mix.

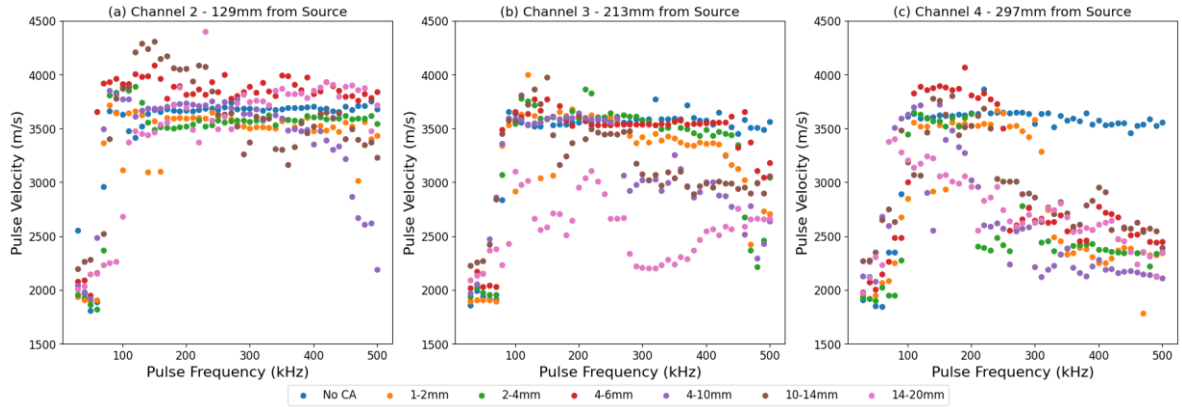

Figure 9 – Individual pulse velocity channels 2, 3, 4 shown by figures (a), (b), (c) respectively. Pulse velocity calculated using time of arrival difference from Channel 1.

The band of low velocity at the start of the plot has been seen in before in frequency dependant testing of concrete and fresh mortar [5][16]. The disparity between the steady velocity above 100 kHz, and the low velocity below 100 kHz could indicate dispersive behaviour. This supports other work by Aggelis et al [17]. Importantly this occurs in all samples, including the one without coarse aggregate. Meaning that it's not a result of the presence coarse aggregate.

The results in Figure 9 show that a narrowband pulse-based autonomous testing system should consider the size and presence of aggregate. As a change of ~3500 m/s to ~2500 m/s would typically be taken as an indication of significant concrete degradation, however in this testing it's seen to occur in undamaged specimens.

4. Conclusion

The behaviour of narrowband ultrasonic pulses between 30-500 kHz was explored for seven specimens distinguished by aggregate size. The attenuation of the high frequency pulses appears to be linked to the size of aggregate. Improved and expanded testing would be required to verify this. The measured change in peak frequency is thought to be a result of high frequency components attenuating faster, leaving behind the lower frequency components, not the result of a genuine frequency shift of the source narrowband pulse. A negative correlation between amplitude loss and frequency was observed. This testing should be expanded to establish if the trend continues up to 1 MHz, taking full advantage of the operating range of the WD sensors and the Conical Transducer source.

Pulse velocity measurements show that for the specimen containing no coarse aggregate, the velocity is independent of the pulse frequency. Whereas all other specimens containing aggregate experienced significant decay of their pulse velocity.

The Red Pitaya and Conical Transducer when used in combination are an effective tool for producing accurate, repeatable narrow-band pulses. As it's fully controllable via code it can produce significantly more data per measurement section than a traditional source methods like impact echo or PLBs. In this testing eight repetitions were done for each frequency pulse. It would be simple to increase this number significantly, potentially providing the large amount of data required for machine learning.

Whilst a separate MISTRAS AE system was used to acquire the data in this testing, the Red Pitaya can do simultaneous input/output. Used extensively in preliminary testing, this capability means it can be used as a standalone pulse and receive system. For these reasons the Red Pitaya shows significant promise for non-destructive autonomous AE testing.

5. Acknowledgements

This research was funded through an ESPRC ICASE Studentship, in collaboration with MISTRAS Group Inc.

6. References

[1] T. Shiotani, K. Hashimoto, N. Okude, C. Granier, K. Watabe, and H. Takamine, 'Assessment of infrastructures by rainy induced AE tomography with wave velocity and attenuation rate', Sep. 2018.

[2] S. L. Gassman and W. F. Tawhed, 'Nondestructive Assessment of Damage in Concrete Bridge Decks', *J. Perform. Constr. Facil.*, vol. 18, no. 4, pp. 220–231, Nov. 2004, doi: 10.1061/(ASCE)0887-3828(2004)18:4(220).

[3] 'Research into the correlation between concrete strength and UPV values'. Accessed: Jun. 25, 2024. [Online]. Available: https://www.ndt.net/article/v09n12/turgut/turgut.htm

[4] J. Y. Park, Y. G. Yoon, and T. K. Oh, 'Prediction of Concrete Strength with P-, S-, R-Wave Velocities by Support Vector Machine (SVM) and Artificial Neural Network (ANN)', *Appl. Sci.*, vol. 9, no. 19, Art. no. 19, Jan. 2019, doi: 10.3390/app9194053.

[5] T. P. Philippidis and D. G. Aggelis, 'Experimental study of wave dispersion and attenuation in concrete', *Ultrasonics*, vol. 43, no. 7, pp. 584–595, Jun. 2005, doi: 10.1016/j.ultras.2004.12.001.

[6] M. F. Kaplan, 'The effects of age and water/cement ratio upon the relation between ultrasonic pulse velocity and compressive strength of concrete', *Mag. Concr. Res.*, vol. 11, no. 32, pp. 85–92, Jul. 1959, doi: 10.1680/macr.1959.11.32.85.

[7] N. HSU and B. FR, 'CHARACTERIZATION AND CALIBRATION OF ACOUSTIC EMISSION SENSORS', *Charact. CALIBRATION Acoust. Emiss. Sens.*, vol. 39, no. 1, pp. 60–68, 1981.

[8] 'Standard Test Method for Measuring the P-Wave Speed and the Thickness of Concrete Plates Using the Impact-Echo Method'. Accessed: Apr. 03, 2024. [Online]. Available: https://compass.astm.org/document/?contentCode=ASTM%7CC1383-04R10%7Cen-US

[9] D. Li, K. Yang, Z. He, H. Zhou, and J. Li, 'Acoustic Emission Wave Velocity Attenuation of Concrete and Its Application in Crack Localization', *Sustainability*, vol. 12, no. 18, Art. no. 18, Jan. 2020, doi: 10.3390/su12187405.

[10] T. Yan, P. Theobald, and B. E. Jones, ‘A self-calibrating piezoelectric transducer with integral sensor for in situ energy calibration of acoustic emission’, *NDT E Int.*, vol. 35, no. 7, pp. 459–464, Oct. 2002, doi: 10.1016/S0963-8695(02)00021-X.
[11] T. Yan, P. Theobald, and B. E. Jones, ‘A conical piezoelectric transducer with integral sensor as a self-calibrating acoustic emission energy source’, *Ultrasonics*, vol. 42, no. 1, pp. 431–438, Apr. 2004, doi: 10.1016/j.ultras.2003.12.039.
[12] M. Eaton, ‘Acoustic Emission (AE) monitoring of buckling and failure in carbon fibre composite structures.’, phd, Cardiff University, 2007. Accessed: Jun. 25, 2024. [Online]. Available: https://orca.cardiff.ac.uk/id/eprint/54625/
[13] A. St-Onge, ‘Akaike information criterion applied to detecting first arrival times on microseismic data’, in *SEG Technical Program Expanded Abstracts 2011*, Society of Exploration Geophysicists, Jan. 2011, pp. 1658–1662. doi: 10.1190/1.3627522.
[14] H. Akaike, ‘Information Theory and an Extension of the Maximum Likelihood Principle’, in *Selected Papers of Hirotugu Akaike*, E. Parzen, K. Tanabe, and G. Kitagawa, Eds., New York, NY: Springer, 1998, pp. 199–213. doi: 10.1007/978-1-4612-1694-0_15.
[15] X. Wu, Q. Yan, A. Hedayat, and X. Wang, ‘The influence law of concrete aggregate particle size on acoustic emission wave attenuation’, *Sci. Rep.*, vol. 11, no. 1, Art. no. 1, 2006, doi: 10.1038/s41598-021-02234-x.
[16] D. G. Aggelis, D. Polyzos, and T. P. Philippidis, ‘Wave dispersion and attenuation in fresh mortar: theoretical predictions vs. experimental results’, *J. Mech. Phys. Solids*, vol. 53, no. 4, pp. 857–883, Apr. 2005, doi: 10.1016/j.jmps.2004.11.005.
[17] D. G. Aggelis, T. P. Philippidis, S. V. Tsinopoulos, and D. Polyzos, ‘Wave Dispersion in concrete due to Microstructure’, 2004.